RESEARCH ARTICLE

Check for updates

Dynamic evolution of Al species in the hydrothermal dealumination process of CHA zeolites†

Benhan Fan,[a,b] Dali Zhu,[a] Linying Wang,[a] Shutao Xu, *[a] Yingxu Wei[a] and Zhongmin Liu [a,b,c]

The hydrothermal stability of zeolites is an important factor being considered as it could restrict their scope of industrial application. Understanding the water-induced dealumination mechanism is crucial for improving the hydrothermal stability of zeolites. Here a series of water-treated H-SSZ-13 samples under hydrothermal conditions was investigated by solid-state NMR methods and we found that dealumination was caused by the hydrolysis of the Al–O bond by water molecules under high temperature and pressure. The hydrolysis of the first Al–O bond could generate framework-associated Al species with a single framework aluminum hydroxyl. The sequential hydrolysis of four Al–O bonds could form the extra-framework aluminum (EFAL) species, which was prone to adsorbing near the Brønsted acid sites (BASs) by electrostatic interaction contributing to stabilizing the molecular sieve framework. Some of the BASs were perturbed by the framework or extra-framework aluminum hydroxyls which was represented by different signals in ^1H MAS NMR due to hydrogen-bonded interactions. The signals between 5 and 8 ppm in ^1H MAS NMR were attributed to the BASs perturbed by framework Al–OH (2.8 ppm), and correspondingly, BASs disturbed by extra-framework Al–OH (2.4 ppm) resulted in the signals appearing between 12 and 15 ppm. These clear attributions were facilitated by ^1H–^1H DQ-SQ and ^1H–^{27}Al S-RESPDOR MAS NMR. More than that, the partial or complete hydrolysis of the framework Al atoms was achieved uniformly by the water-treatment process under conditions of high temperature and pressure.

[a]*National Engineering Research Center of Lower-Carbon Catalysis Technology, Dalian National Laboratory for Clean Energy, iChEM (Collaborative Innovation Center of Chemistry for Energy Materials), Dalian Institute of Chemical Physics, Chinese Academy of Sciences, Dalian 116023, China. E-mail: xushutao@dicp.ac.cn*
[b]*University of Chinese Academy of Sciences, Beijing 100049, P. R. China*
[c]*State Key Laboratory of Catalysis, Dalian Institute of Chemical Physics, Chinese Academy of Sciences, Dalian 116023, P.R. China*
†Electronic supplementary information (ESI) available. See DOI: https://doi.org/10.1039/d2qi00750a

Introduction

Zeolites have extensive applications in many fields such as the petrochemicals industry, separation and ion exchange processes due to their well-defined crystalline structures, high surface area, variable acid strength and appropriate hydrothermal stability.[1] Nowadays, multitudinous zeolites have unquestionably become the backbone of the petrochemicals industry in diverse prominent catalytic reactions: for instance, FAU-type zeolites are widely used in fluid catalytic cracking (FCC);[2] CHA-type zeolites are applied for the methanol-to-olefin (MTO) reactions;[3,4] MFI-type zeolites can promote methanol-to-propene (MTP) or methanol-to-gasoline (MTG) processes;[5–7] MOR-type zeolites are employed for dimethyl ether (DME) carbonylation and so forth.[8,9] The catalytically active center is the so-called Brønsted acid site (BAS), a hydroxyl group bridging aluminum and silicon, generated by substituting a Si with an Al atom and the negative charge compensated by a proton.[10] Hydrothermal stability is a critical factor that needs to be considered in the application of zeolites because many reactions are accompanied by the introduction and generation of water in real conditions. Water molecules inevitably interact with the framework Al atoms and the degree of effects from weak to strong could be divided into adsorption,[11] reversible hydrolysis[12–14] and irreversible hydrolytic removal of framework Al atoms that form the extra-framework aluminum species (EFALs).[15]

Water-treatment-induced dealumination is a double-edged sword. Continuous dealumination permanently reduced the active sites (here the BASs) resulting in deactivation. On the other hand, appropriate dealumination could adjust the Si/Al ratio and improve the hydrothermal stability, for example, high-temperature hydrothermal dealuminated ultra-stable Y (USY) zeolites that are widely used in the FCC process.[2] So a

This journal is © the Partner Organisations 2022

Inorg. Chem. Front., 2022, **9**, 3609–3618 | **3609**

better understanding of the dealumination process may help in finding a favorable zeolite with excellent hydrothermal stability for further industrial applications. How water molecules interact with the framework Al T-site at the atomic level is a key scientific question, but it is also a challenge for experimental research. Nevertheless, theoretical calculation is very helpful to explore the water interactions considering multiple factors at the molecular level, such as the number of water molecules, multifarious zeolite topologies and specific T-sites.[16–19] Among the zeolites, the CHA-type zeolites are a suitable candidate for both theoretical and experimental studies and they have been most studied due to their relatively simple crystallographic structure, particularly that of one T-site and four O-sites.[12,16,17,19–22] The dealumination process of the zeolite originates from the hydrolysis of the first Al–O bond, and then the sequential breakage of the remaining three Al–O bonds generates EFAL and silanol nests. The first detailed dealumination pathway of H-CHA with a single water molecule effect wasproposed.[16] A subsequent mechanism in which a single water molecule bonds with an Al atom at the anti-site of a BAS was put forward, then a 1,2 water dissociation acted on the Al–O bond and led to its rupture accompanied by the formation of a new BAS.[17,19] The mechanism of multimolecular water dissociation was gradually mentioned in the following years.[18,23] More than that, more detailed work directed at H-SSZ-13 has been explored such as the kinetics of dealumination[21] and the effects of adjacent Al atoms on hydrothermal stability.[24] The Al pairs in the H-SSZ-13 are the key factors that affect hydrothermal stability.[25] The first-principles calculation method proved that Al pairs tended to occupy the *para*-sites of the 4MRs. The second Al atom in the *para*-site can be easily removed once the framework loses the first one. The dealumination of Al pairs would break the linker of 6MRs in the framework, which is responsible for the degraded hydrothermal stability.[24]

Notwithstanding what extensive and detailed theoretical computational work has demonstrated, the experimental investigations of molecular sieve dealumination are catching up as well. Diversiform characterization methods, such as diffuse reflectance infrared Fourier transform spectroscopy (DRIFTS),[26,27] solid-state nuclear magnetic resonance (ssNMR),[15,28,29] synchrotron-based pair distribution function (PDF) analysis,[30] synchrotron radiation powder X-ray diffraction (SR-PXRD)[27,31] and X-ray absorption spectroscopy (XAS)[31–33] were synergistically combined to explore the species that were generated accompanying the removal of framework aluminum. Al species in zeolites are multifarious and can be divided into framework, framework-associated and extra-framework aluminum.[34–38] The composition of EFAL species is very complex and they are composed of oxides and multiple hydroxides, of which some are neutral species such as $Al(OH)_3$, $AlOOH$, Al_2O_3 or multinuclear clusters, and others are species with electric charges such as AlO^+, $Al(OH)_2^+$ and $Al(OH)^{2+}$.[39–43] According to the different coordination numbers of Al species, EFAL can also be divided into three-coordinated, tetrahedral coordinated, distorted tetrahedral coordinated, five-coordinated

and octahedral aluminum.[42,44–46] Identical Al species may overlap in different classifications. More than that, some structures of notable Al species have been posited, but the suitability of each in matching the experimental data has not been assessed. It is worth noting that the identification of Al species is of great significance for decoding the effect of water interacting with the zeolite framework and deepening our understanding of the inherent hydrothermal stability.

Solid-state NMR is a powerful tool to provide structural information about zeolites. ^1H and ^{27}Al magnetic angle spinning (MAS) NMR could help to distinguish different hydroxyl groups and different coordination states of Al species; more than that, the spatial proximity of hydroxyl and Al in different coordination states could be further mapped by ^1H and ^{27}Al double quantum (DQ) MAS NMR.[41,42] Two-dimensional NMR spectroscopy, such as ^{27}Al multiple-quantum (MQ) MAS NMR[37,47] and insensitive nuclei enhancement by polarization transfer (INEPT),[44] can shed light on the inconclusive aluminum structure and help to elucidate the coordination state. Introducing probe molecules such as trimethylphosphine (TMP) may also change the coordination state of the concerned Al species to achieve accurate identification by ^{31}P MAS NMR or ^{27}Al–^{31}P INEPT spectroscopy.[44,48]

In this work, a series of elaborately prepared autoclave hydrothermally treated SSZ-13 samples was adopted to explore the dynamic evolution of Al species in the dealumination process. One-dimensional ^1H, ^{27}Al and ^{29}Si MAS NMR combined with ^1H–^1H DQ-SQ and ^1H–^{27}Al S-RESPDOR methods precisely revealed the detailed structures of Al species generated by water treatment. The complete dealumination mechanism is helpful to understand in depth the interaction between water molecules and the zeolite framework, and then interpret the intrinsic hydrothermal stability of molecular sieves.

Experimental section

Materials and methods

The Na^+-free SSZ-13 (Si/Al = 12.5) was synthesized hydrothermally using a modified method developed in our previous work.[49,50] H-SSZ-13 was obtained by calcination from the as-synthesized parent Na^+-free SSZ-13, and then dehydrated under vacuum (<10^{-5} Pa) at 773 K for more than 12 h. After dehydration, the samples were transferred into a glovebox under an Ar environment for post-treatment. Dehydrated H-SSZ-13 (100 mg) was added into a quartz tube combined with different volumes of water which was introduced by a microinjector. Finally, the quartz tube was placed into a tailor-made stainless autoclave (Fig. S1 and S2†) and then heated at 573 K for 6 h in the muffle furnace. The samples were named H-SSZ-13-*X* (*X* represented the total volume of water during the water-treatment process). It is worth noting that H-SSZ-13–40 and H-SSZ-13–80 represent samples in which 20 μL of water was added each time and the hydrothermal treatment was performed two and four times, respectively.

All the ^{1}H, ^{27}Al and ^{29}Si experiments were performed on a Bruker Avance III 600 spectrometer equipped with a 14.1 T and 89 mm wide-bore magnet using a 3.2 mm HXY triple resonance MAS probe with the corresponding Larmor frequencies of 600.13, 156.5 and 119.2 MHz, respectively. The chemical shifts were referenced to adamantane $[\delta(^{1}H) = 1.74\ \text{ppm}]$, 1 M Al(NO$_3$)$_3$ solution $[\delta(^{27}Al) = 0\ \text{ppm}]$ and kaolinite $[\delta(^{29}Si) = -91.5\ \text{ppm}]$. The samples were dehydrated under vacuum (not higher than 10^{-3} Pa) at 773 K for 12 h to remove the physically adsorbed water and then transferred into a glovebox under an Ar environment in order to fill the ZrO$_2$ rotors with Kel-F caps for further NMR measurements with dehydration requirements such as ^{1}H MAS NMR, ^{1}H–^{1}H DQ-SQ MAS NMR, ^{1}H–^{29}Si HETCOR and ^{1}H–^{27}Al S-RESPDOR. Detailed descriptions of the synthesis, post-treatment and characterization methods are listed in the ESI.†

Results and discussion

Structural transformations induced in the SSZ-13 framework during rigorous water treatment

Herein, a series of H-SSZ-13 treated with different volumes of water was meticulously characterized by SEM and XRD methods (Fig S4 and S5†). The results of the untreated H-SSZ-13 sample showed a dominating homogeneous CHA phase with a size of 2–3 μm. With the introduction of a small amount of water, the two noteworthy samples, H-SSZ-13–5 and H-SSZ-13–10, still maintained the typical CHA structure with small particles which were possibly amorphous dealuminated species on the surface of the zeolite. With the increase of water injection, macroscopic defects appeared on the surface of H-SSZ-13–20, 40 and 80 which proved the dealumination process occurred apparently with the increase of water. It could be seen from XRD patterns that although the content of water is increasing, the topological structure of H-SSZ-13 is still maintained and the morphology of the samples also remained unchanged which was clear in the SEM photographs.

^{27}Al MAS NMR (Fig. 1a) is a powerful tool to monitor the evolution of Al species during the hydrothermal process. The main signal around 59 ppm in the parent H-SSZ-13 was assigned to the framework tetrahedrally coordinated Al(IV) and the tiny signal at 0 ppm was attributed to the octahedrally coordinated Al(VI), so-called EFAL, which could not escape on being generated in the process of deammoniation.[51] As the amount of water increased, the intensity of the main signal at 59 ppm gradually decreased, and simultaneously, a new broad signal around 47 ppm gradually emerged and increased along with the signal at 0 ppm. ^{27}Al is a spin 5/2 nucleus, so the second-order quadrupole interactions will affect the analysis of one-dimensional ^{27}Al MAS NMR. To better distinguish different Al species, ^{27}Al MQ MAS NMR (Fig. 1b and c) was adopted for a deeper understanding of the two most relevant samples, the parent H-SSZ-13 and water-treated H-SSZ-13–80. In the parent H-SSZ-13, there are only two signals in the ^{27}Al
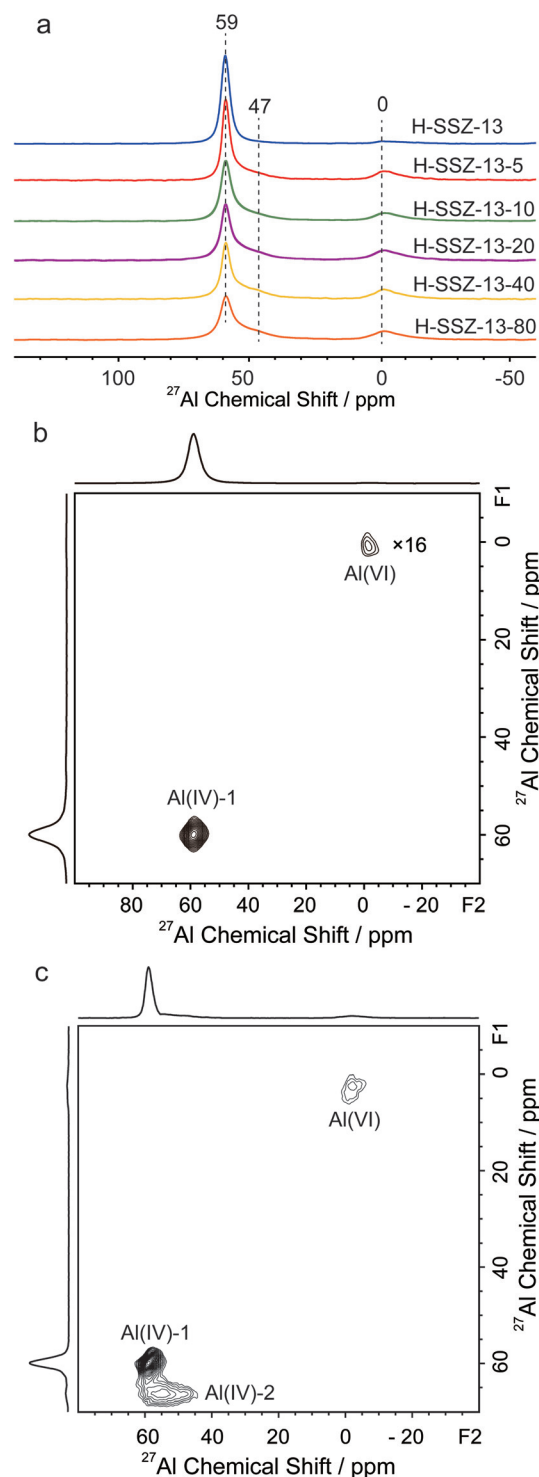

Fig. 1 (a) ^{27}Al MAS NMR spectra of parent H-SSZ-13 and a series of water-treatment H-SSZ-13-X (X = 5, 10, 20, 40 and 80); ^{27}Al MQ MAS spectra of H-SSZ-13 (b) and H-SSZ-13–80 (c). All the samples were hydrated.

MQ spectra. The main signal was ascribed to the framework tetrahedrally coordinated Al(IV), and the other signal was assigned to the octahedrally coordinated Al(VI) with an intensity that was amplified 16 times as shown in the spectra.

This journal is © the Partner Organisations 2022

Inorg. Chem. Front., 2022, **9**, 3609–3618 | **3611**

Besides the two signals above, a new signal with a large quadrupole coupling constant (C_q) appeared in the sample H-SSZ-13–80. The attribution of this signal is still in dispute, and a similar signal was observed in dealuminated mordenite zeolite and assigned to distorted tetrahedrally coordinated Al by ^{27}Al MQ MAS NMR.[52] Subsequently, Deng's group investigated dealuminated HY zeolite and attributed this parallel signal (Al[IV], b) to four-coordinated EFAL (AlOH[2+]) species by combining ^{27}Al DQ, ^{27}Al MQ MAS NMR and DFT calculations.[42] However, in recent years, this analogous signal of Al (IV)-2 appeared in the ^{27}Al MQ MAS NMR spectra following a mild steam treatment of ZSM-5 zeolites and vanished on ammonium hexafluorosilicate (AHFS) washing. Utilizing ultra-high field (35.2 T) 2D [1]H–^{27}Al correlation and MQ MAS NMR experiments, hydrated and dehydrated samples were both considered, revealing that the signal of Al(IV)-2 was derived from the partially coordinated framework $(SiO)_{4-n}Al(OH)_n$ species.[35,36] So in this work, the broad signal appeared at 47 ppm in ^{27}Al MAS NMR and the corresponding signal with a large C_q in ^{27}Al MQ MAS NMR was attributed to the partially coordinated framework Al species which were denoted as Al (IV)-2, and correspondingly, the well-known framework tetrahedrally coordinated Al(IV) was denoted as Al(IV)-1 which are marked in Fig. 1. Moreover, the Al(IV)-2 species possibly resulted from crystal defects or the partial hydrolysis of the framework Al–O bond, which is believed to be the precursor of the EFAL species.[35] Considering the actual water treatment process in this work, Al(IV)-2 species did not exist in the parent H-SSZ-13 and gradually appeared accompanying the introduction of water, it could be ruled out that this signal did not come from the defects of the parent zeolite but from the incomplete hydrolysis of the Al–O bond. At the same time, EFALs were irreversibly generated by the thorough hydrolysis of the four Al–O bonds during the process of water treatment.

To further study the interaction site between water and the framework, ^{29}Si MAS NMR (Fig. 2a) combined with ^{1}H MAS NMR (Fig. 3) was performed to describe the evolution of Si species and hydroxyl species in the hydrothermal processes. All the samples represented three primary signals at −101, −105 and −111 ppm from low field to high field as shown in Fig. 2a. Considering the chemical shift value, the signal at −101 ppm was preliminarily attributed to Q3 $Si(O–Si)_3(OH)$ silanol groups or $Si(O–Si)_2(O–Al)_2$. The distinct signal (−101 ppm) was significantly enhanced in the [1]H–[29]Si cross polarization (CP) MAS NMR spectrum compared with ^{29}Si MAS NMR spectrum, suggesting that it should be assigned to Q3 silanol groups rather than $Si(O–Si)_2(O–Al)_2$ sites. Correspondingly, −105 ppm represented $Si(O–Si)_3(O–Al)$ and −111 ppm belonged to Q4 $Si(O–Si)_4$ sites.[53,54] In the 2D ^{1}H–^{29}Si CP-HECTOR MAS NMR spectrum (Fig. 2c), three signals (−101, −105 and −111 ppm) were shown in the projection of the [29]Si dimension. Two well-separated signals at 1.6 and 3.8 ppm were displayed in the ^{1}H dimension, which also appeared in the following ^{1}H MAS NMR (Fig. 3a), which were credibly attributed to protons in silanols (Si–OH) and bridging hydroxyl groups of BAS, respectively.[51,55] So the two strong cor-
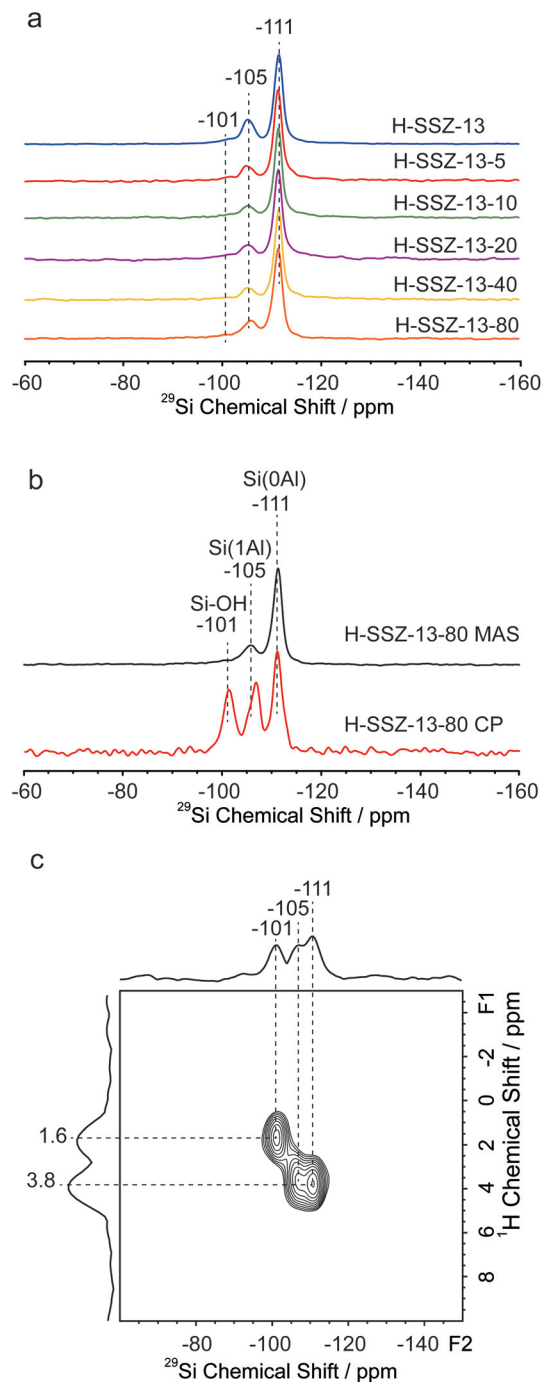

Fig. 2 (a) ^{29}Si MAS NMR spectra of parent H-SSZ-13 and a series of water-treatment H-SSZ-13-*X* (*X* = 5, 10, 20, 40 and 80); (b) ^{29}Si MAS NMR, ^{1}H–^{29}Si CP NMR spectra of H-SSZ-13–80; (c) [1]H–[29]Si CP HETCOR spectrum of H-SSZ-13–80, the sample H-SSZ-13–80 for [1]H–^{29}Si CP and CP-HETCOR MAS NMR spectra were dehydrated at 773 K under vacuum condition. The contact time of CP and HETCOR experiments are both 2 ms.

related peaks at (1.6, −101) and (3.8, −105) could indicate the close spatial proximity of Si–OH and Si(1Al) species. The remaining correlated signal at (3.8, −111) is due to the long contact time (2 ms) for the CP MAS NMR experiment which
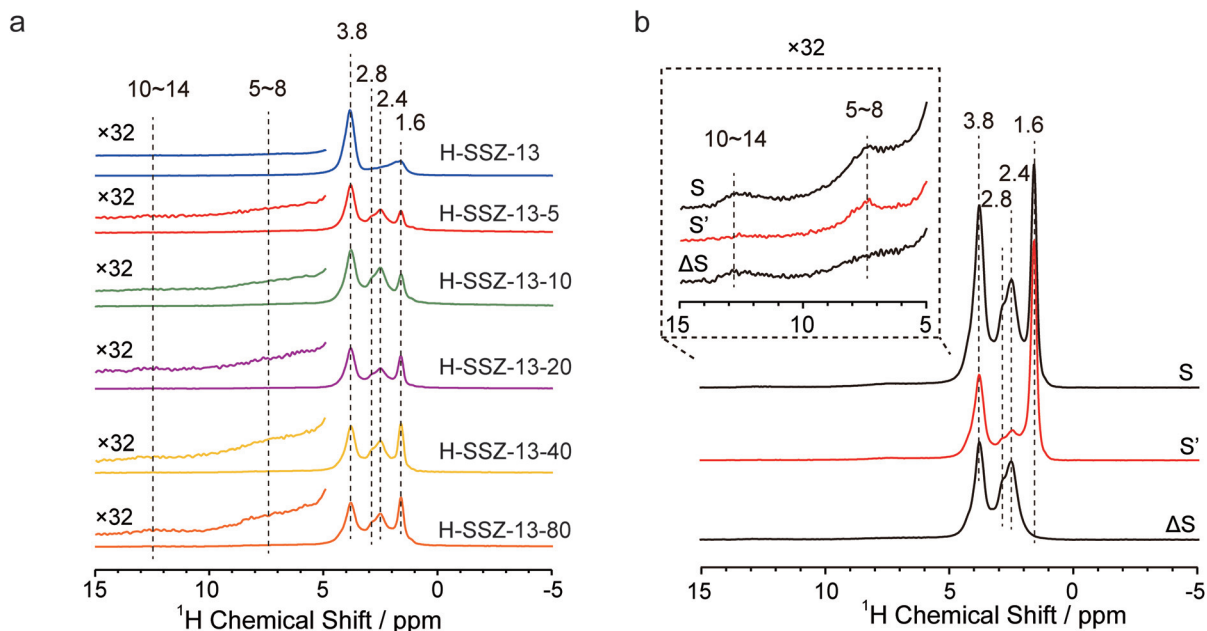
Fig. 3 (a) ^{1}H MAS NMR spectra of parent H-SSZ-13 and a series of water-treatment H-SSZ-13-X (X = 5, 10, 20, 40 and 80); (b) ^{1}H–^{27}Al S-RESPDOR spectra of H-SSZ-13–80 with (S') and without (S) ^{27}Al irradiation with a recoupling time of 0.4 ms. ΔS is the difference spectrum between S and S'. All the samples were dehydrated at 773 K under vacuum conditions.

could transfer the polarization of protons in the BAS to the adjacent Q4 $Si(O–Si)_4$ species in the dehydrated sample. It is worth noting that compared with the parent H-SSZ-13, the intensity of Si(1Al) signals showed a significant decrease after water-treatment which indicated that BAS is a preferential site of interaction between water molecules and the molecular sieve framework.

The identification of hydroxyl species played a crucial role in the evolution of the zeolite framework which ^{1}H MAS NMR could demonstrate by the detailed information about the dehydrated samples as shown in Fig. 3a. Four distinct signals appeared in all the samples, of which two signals at 1.6 and 3.8 ppm have been explained in detail above. The other two signals at 2.4 and 2.8 ppm were attributed to aluminum hydroxyls (Al–OH).[55] In the parent H-SSZ-13, the dominant signal is the bridging hydroxyl generated from Al atoms incorporated into the zeolite framework. The proportion of Si–OH and Al–OH was not obvious, and the Si–OH group was most likely generated from the terminal hydroxyl or defect sites caused by inevitable dealumination during the calcination process. The Al–OH signal generated by dealumination is mainly at 2.4 ppm, and the intensity of signal at 2.8 ppm could be neglected. Considering the state of the original H-SSZ-13 with the vast majority of framework Al and a few extra-framework Al species which were detected by ^{27}Al MAS NMR, the 2.4 ppm peak could be credibly ascribed to extra-framework Al–OH. As the amount of added water increased, a consistent trend could be found that the intensity of BAS gradually declined along with the increase of the Al–OH and Si–OH species. This phenomenon indicated that the introduction of water will act

on the BAS and hydrolyze the Al–O bond. The hydrolysis process was accompanied by the reduction of BAS content and the formation of EFALs, resulting in more defects and the formation of supernumerary Al–OH and Si–OH species. More than that, the two broad signals at 5–8 ppm and 10–14 ppm did not exist in the parent H-SSZ-13 but appeared in the remaining samples. The intensity of the two signals varied with the amount of water which means that these two kinds of protons were generated from the water treatment processes.

Identification of aluminum hydroxyls generated after dealumination

The signals at 2.4 and 2.8 ppm in the ^{1}H NMR had been commonly observed in the H-SSZ-13 and roughly assigned to Al–OH moieties of EFALs.[51,56] It is still unknown whether these two signals were the same species caused by different local environments or different hydroxyl species, and there is a lack of experimental evidence. To determine the spatial distance relationship between different hydroxyl and aluminum species, the ^{1}H–^{27}Al symmetry-based rotational-echo saturation-pulse double-resonance (S-RESPDOR) method was adopted to explore the H-SSZ-13–80 as shown in Fig. 3b. Two ^{1}H MAS NMR spectra with (S') and without (S) ^{27}Al irradiation were acquired comparatively. If the concerned signal showed fast decay with ^{27}Al irradiation, it could be concluded that the strong ^{1}H–^{27}Al dipolar couplings existed between ^{1}H and ^{27}Al spins, indicating spatial proximities between protons and Al species. In other words, the signals that appeared in the difference spectrum (ΔS) by subtraction of S and S' could be noticed which is mainly due to the dephasing effects induced by

^{1}H–^{27}Al dipole–dipole interaction. Just as expected, the signals of BAS and two aluminum hydroxyl groups decayed, and in contrast, there was no change in the peak of Si–OH. Unexpectedly, two broadened signals between 5–8 ppm and 10–14 ppm also appeared in the difference spectrum, which means that these two types of protons were close to the Al species. Moreover, these two signals did not appear in the original H-SSZ-13, and instead, arose with the increase of two aluminum hydroxyl groups. Therefore, it was speculated that these two kinds of protons are presumably related to the most relevant aluminum hydroxyl groups.

The two-dimensional ^{1}H–^{1}H DQ MAS NMR method had been demonstrated as an effective method that could be competent to detect proton–proton proximity (<5 Å) in dealuminated zeolites.[41] Since various protons of hydroxyl groups were observed in ^{1}H MAS NMR, ^{1}H–^{1}H DQ MAS NMR had been employed to detect the spatial proximities among various hydroxyl groups in the parent H-SSZ-13 and H-SSZ-13–80 as shown in Fig. 4. Signals that appeared along the diagonal were the autocorrelation peaks (ω, 2ω) which resulted from the dipolar interaction of protons of the same species. Paired signals (ω_a, $\omega_a + \omega_b$) and (ω_b, $\omega_a + \omega_b$) that appeared off-diagonal were the correlations between two protons of the different species. Two autocorrelation peaks and one off-diagonal peak pair could be observed in the sample of the parent H-SSZ-13. The one autocorrelation peak appearing at (1.6, 3.2) ppm suggested the spatial proximity of silicon hydroxyl groups. The other autocorrelation peak at (3.8, 7.6) ppm indicated that spatial proximity of BAS might exist in the parent SSZ-13 because the silica–alumina ratio was 12.5 indicating that one CHA cage has an average of one BAS.[53,57] The off-diagonal peak pair at (2.4, 6.2) and (3.8, 6.2) ppm corresponded to the correlation between BAS and Al–OH and this phenomenon could be attributed to the spatial proximity of BAS and extra-framework Al–OH groups which was inevitably generated in the calcinating process. After the hydrothermal treatment, the ^{1}H–^{1}H DQ MAS NMR spectrum became more complex. However, the identical two autocorrelation peaks (1.6, 3.2) and (3.8, 7.6) along with paired (2.4, 6.2) and (3.8, 6.2) ppm were observed in the parent H-SSZ-13, and one autocorrelation peak and three off-diagonal peak pairs were clearly observed and discussed in detail later. The first off-diagonal peak pair at (2.4, 5.2) and (2.8, 5.2) ppm corresponded to the correlation of extra-framework Al–OH and newly generated Al–OH groups. The second off-diagonal peak pair at (2.4, 14.6–16.0) and (12.2–13.6, 14.6–16.0) ppm represented the correlation between 2.4 ppm and the generated broad signal (approximately at 10–14 ppm) in the ^{1}H–^{27}Al S-RESPDOR. The production of this new signal had the consequent relationship with the extra-framework Al–OH. The analogous broad signal that appeared at 12–15 ppm in ^{1}H NMR of MFI-type zeolite was first reported and attributed by Chen and co-workers. This signal was attributed to the BAS which was perturbed by hydroxyls on extra-lattice aluminum species characterized by ^{1}H MAS NMR and ^{1}H 2D-exchange MAS NMR experiments along with the alkane probe molecule of isobutane.[58] And in this work, the broad signal at 10–14 ppm could stand for the same perturbed BAS species which was affected by extra-framework Al–OH with the signal at 2.4 ppm. The third off-diagonal peak pair at (2.8, 8.4–11.2) and (5.6–8.4, 8.4–11.2) ppm corresponded to the correlation of the new generated Al–OH groups (2.8 ppm) and another broad signal (5–8 ppm) which was adjacent to Al species in the ^{1}H–^{27}Al S-RESPDOR. The ^{1}H signal at 2.8 ppm was relevant to the Al(IV)-2 species in ZSM-5 zeolite mainly because of the evidence of the correlation peak in the ^{1}H–^{27}Al D-HMQC experiments at high fields such as 19.6 and 35.2 T.[35] This Al(IV)-2 species was incontrovertibly demonstrated to be the partially bonded framework $(SiO)_{4-n}Al(OH)_n$

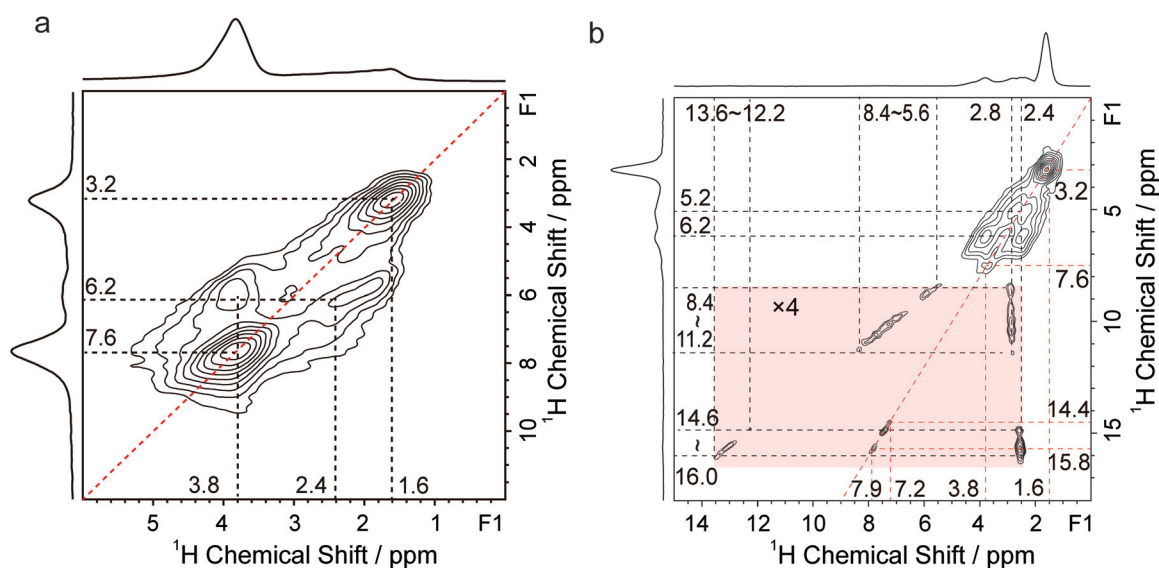**Fig. 4** (a) ^{1}H–^{1}H DQ MAS NMR spectra of parent H-SSZ-13 (a) and H-SSZ-13–80 (b) with the sample dehydrated.

3614 | *Inorg. Chem. Front.*, 2022, **9**, 3609–3618

This journal is © the Partner Organisations 2022

species by multi NMR methods at the ultrahigh field (35.2 T).[35,36] And back to the off-diagonal peak pair at (2.8, 8.4–11.2) and (5.6–8.4, 8.4–11.2) ppm in the ^1H–^1H DQ-SQ spectra (Fig. 3b), the broad signal which appeared at 5–8 ppm was unequivocally attributed to the perturbed BAS by framework Al–OH species.[35,36] Moreover, the autocorrelation peak (7.2–7.9, 14.4–15.8) also represented the spatial proximity of this kind of perturbed BAS. Because there was no observation of an autocorrelation peak at (2.8, 5.6) ppm, the 2.8 ppm peak was further ascribed to the framework $(SiO)_3Al(OH)$ species.

Mechanism of water-induced dealumination on SSZ-13

Understanding the dealumination mechanism of molecular sieves is of great importance to improve hydrothermal stability. Previous studies of the stability of zeolites under a water atmosphere, especially the DFT calculation, are helpful for a deeper understanding of the acquired NMR data. The first detailed reaction paths for step-by-step dealumination of CHA type zeolite were carefully described by the method of DFT calculation.[16] The Si–O–Al bond was hydrolyzed by the first member of water with the formation of a vicinal disilanol defect, and then the first Al–O bond thoroughly breaks down with the new generated Si–OH and the framework Al–OH accompanied by a changed position of BAS. As the number of water molecules increased to three, the intermediate of $Al(OH)_3$ species was formed with two hydrogen bonds to the framework, and the fourth water molecule was crucial for removing the EFAL species, the so-called new generated $Al(OH)_3(H_2O)$ intermediate, from the framework. Subsequent work was concentrated on the first Al–O bond hydrolysis and put forward a new pathway by periodic DFT calculation.[17] The first water was absorbed on the anti-position to BAS, and subsequent 1,2-dissociation of water on proximal oxygen with concomitant axial bond breaking, leading to a partial dislodgement of framework Al and reversible recovery of BAS. This new mechanism seems more plausible than the previous one which means that the activation energy of the first Al–O bond breaking (76 kJ mol^{-1}) was much lower than the "vicinal disilanol" intermediate induced pathway (190 kJ mol^{-1}) in the CHA type zeolite. The possible intermediate structure resulting from the first Al–O bond breaking though was represented and could help to understand the full-path hydrolysis of zeolite.

Based on our experiment data, this intermediate framework $(SiO)_3Al(OH)$ was undoubtedly observed and characterized. As a result, the proposed full-path mechanism of the dealumination process induced by rigorous hydrothermal treatment of H-SSZ-13 zeolite is shown in Scheme 1. The dealumination of the molecular sieves originated from the rupture of the first Al–O bond, and the first water molecule preferentially adsorbed in the opposite framework Al position toward BAS, forming a distorted tetrahedral coordinated or five-coordinated Al species. And then the 1,2-dissociation of water on the neighboring framework O atom, with corresponding axial Si–O bond breaking, generated a new Si–OH. At the same time, the absent BAS was recovered at the adjacent O site along with a new generated framework Al–OH. This framework Al–OH
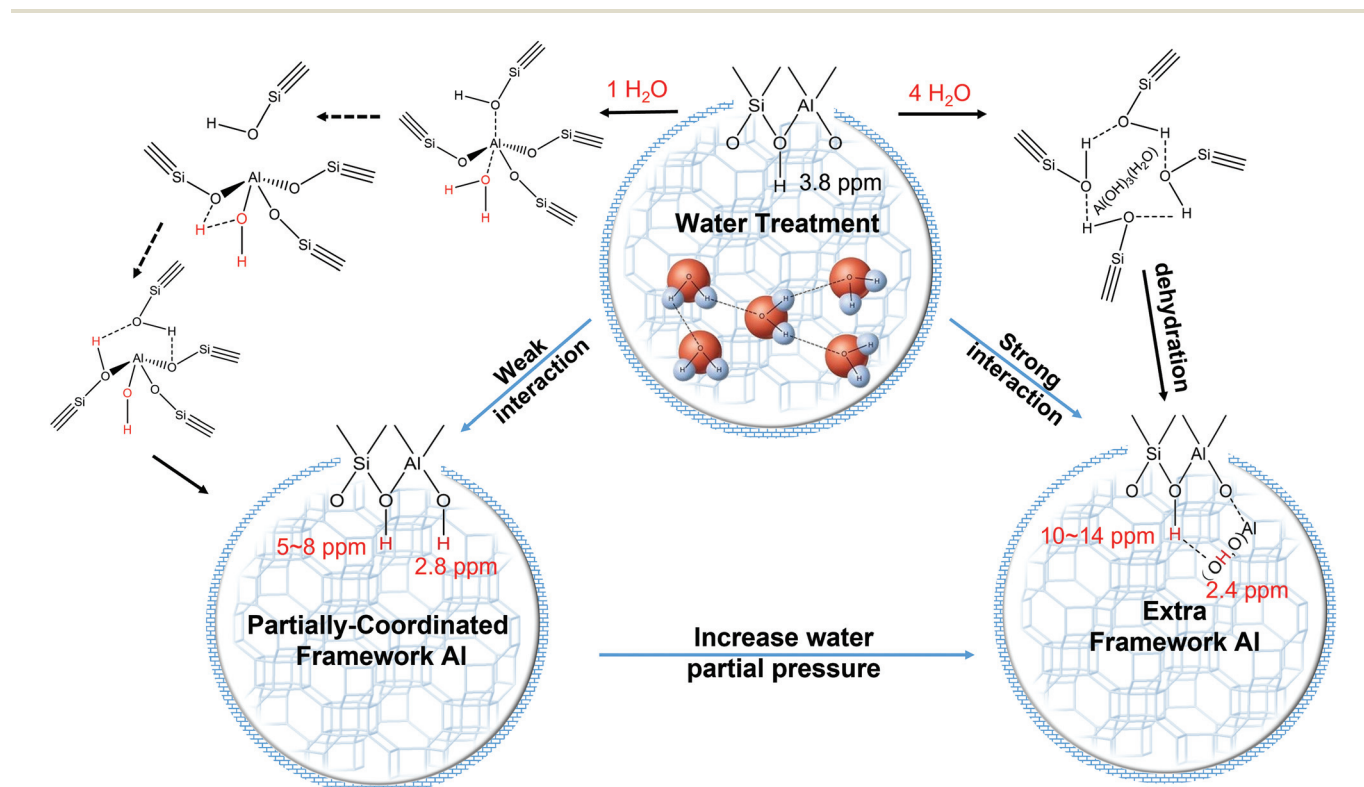
Scheme 1 Proposed mechanism of dealumination process induced by hydrothermal-treatment of SSZ-13 zeolite.

with the ^1H signal at 2.8 ppm could perturb the proximal BAS and caused the ^1H chemical shifts to appear approximately at 5–8 ppm. After the treatment of monomolecular water, the second and third water also adopted an analogical pattern forming the $(SiO)_2Al(OH)_2$ and $(SiO)Al(OH)_3$ species, respectively. The fourth water was crucial for the formation of the EFAL species by completely breaking the only remaining Al–O bond generated by the $Al(OH)_3(H_2O)$ and silicon hydroxyl nests. These $Al(OH)_3(H_2O)$ or congeneric extra-framework Al–OH moieties transferred into the extra-framework aluminum oxygen species that were prone to adsorbing near the BAS by electrostatic interaction and contributed to stabilizing the molecular sieve framework. Moreover, these hydroxyls on extra-lattice aluminol species with the ^1H signal at 2.4 ppm could perturb the proximal BAS and caused the ^1H chemical shifts to appear approximately at 10–14 ppm. These monomolecular or polymolecular water hydrolysis routes were simultaneous under rigorous hydrothermal treatment. So under high temperature and pressure, the water molecules became more free and dispersed. The partially coordinated framework Al was generated in places with low concentrations of water, and in contrast, the EFAL species were easily produced under a high concentration of water.

Conclusions

In this study, the CHA-type zeolite with hydrothermal treatment had been investigated in detail using 1D and 2D solid-state NMR methods. The intermediate Al–OH species generated under the water atmosphere were elaborately characterized by ^1H–^1H DQ-SQ and ^1H–^{27}Al S-RESPDOR NMR methods. The ^1H signals of 2.4 ppm and 2.8 ppm were demonstrated to be extra-framework Al–OH and framework Al–OH respectively. These two kinds of hydroxyl species could perturb the adjacent BAS and shift the chemical shift to the lower field. The signals between 5 and 8 ppm in ^1H MAS NMR were attributed to BAS perturbed by framework Al–OH, and correspondingly, the extra-framework Al–OH disturbed BAS appeared between 12 and 15 ppm. These two species also revealed different pathways of dealumination mechanisms. The partially coordinated framework Al species was generated by the monomolecular water-induced hydrolysis reaction in which one water molecule attacked the anti-position of the Al atom toward the BAS resulting in the first Al–O bond breaking. Extra-framework Al species were generated by stepwise hydrolysis of four Al–O bonds which needed at least four molecules of water. These two kinds of dealumination mechanisms took place simultaneously under the conditions of hydrothermal treatment of the SSZ-13 zeolite. The detailed experimental evidence of intermediates for different dealumination pathways was given in this work. Through these two intermediates, the whole process from the first Al–O bond breaking to the complete hydrolysis of four Al–O bonds results in EFALs which could be better understood at the atomic level. Moreover, it would help to reveal the intrinsic hydrothermal stability of molecular sieves.

Author contributions

The manuscript was written through contributions of all authors. All authors have given approval to the final version of the manuscript.

Conflicts of interest

The authors declare no competing financial interest.

Acknowledgements

References

1 A. Corma, From microporous to mesoporous molecular sieve materials and their use in catalysis, *Chem. Rev.*, 1997, **97**, 2373–2419.

2 E. T. C. Vogt and B. M. Weckhuysen, Fluid catalytic cracking: recent developments on the grand old lady of zeolite catalysis, *Chem. Soc. Rev.*, 2015, **44**, 7342–7370.

3 P. Tian, Y. Wei, M. Ye and Z. Liu, Methanol to olefins (MTO): From fundamentals to commercialization, *ACS Catal.*, 2015, **5**, 1922–1938.

4 M. Yang, D. Fan, Y. Wei, P. Tian, Z. Liu, M. Yang, D. Fan, Y. Wei, P. Tian and Z. Liu, Recent progress in methanol-to-olefins (MTO) catalysts, *Adv. Mater.*, 2019, **31**, 1902181.

5 M. Stöcker, Methanol-to-hydrocarbons: catalytic materials and their behavior, *Microporous Mesoporous Mater.*, 1999, **29**, 3–48.

6 J. F. Haw, W. Song, D. M. Marcus and J. B. Nicholas, The mechanism of methanol to hydrocarbon catalysis, *Acc. Chem. Res.*, 2003, **36**, 317–326.

7 U. Olsbye, S. Svelle, M. Bjrgen, P. Beato, T. V. W. Janssens, F. Joensen, S. Bordiga and K. P. Lillerud, Conversion of methanol to hydrocarbons: how zeolite cavity and pore size controls product selectivity, *Angew. Chem., Int. Ed.*, 2012, **51**, 5810–5831.

8 P. Cheung, A. Bhan, G. J. Sunley and E. Iglesia, Selective carbonylation of dimethyl ether to methyl acetate catalyzed by acidic zeolites, *Angew. Chem., Int. Ed.*, 2006, **45**, 1617–1620.

9 E. Zhan, Z. Xiong and W. Shen, Dimethyl ether carbonylation over zeolites, *J. Energy Chem.*, 2019, **36**, 51–63.

10 W. O. Haag, R. M. Lago and P. B. Weisz, The active site of acidic aluminosilicate catalysts, *Nature*, 1984, **309**, 589–591.

11 L. Smith, A. K. Cheetham, R. E. Morris, L. Marchese, J. M. Thomas, P. A. Wright and J. Chen, On the nature of water bound to a solid acid catalyst, *Science*, 1996, **271**, 799–802.

3616 | *Inorg. Chem. Front.*, 2022, **9**, 3609–3618

This journal is © the Partner Organisations 2022

12 C. J. Heard, L. Grajciar, C. M. Rice, S. M. Pugh, P. Nachtigall, S. E. Ashbrook and R. E. Morris, Fast room temperature lability of aluminosilicate zeolites, *Nat. Commun.*, 2019, **10**, 1–7.

13 S. M. Pugh, P. A. Wright, D. J. Law, N. Thompson and S. E. Ashbrook, Facile, Room-temperature 17O enrichment of zeolite frameworks revealed by solid-state NMR spectroscopy, *J. Am. Chem. Soc.*, 2020, **142**, 900–906.

14 T. Sun, S. Xu, D. Xiao, Z. Liu, G. Li, A. Zheng, W. Liu, Z. Xu, Y. Cao, Q. Guo, N. Wang, Y. Wei and Z. Liu, Water-induced structural dynamic process in molecular sieves under mild hydrothermal conditions : ship-in-a-bottle strategy for acidity identification and catalyst modification, *Angew. Chem.*, 2020, **132**, 20672–20681.

15 R. M. Ravenelle, F. Schübler, A. Damico, N. Danilina, J. A. Van Bokhoven, J. A. Lercher, C. W. Jones and C. Sievers, Stability of zeolites in hot liquid water, *J. Phys. Chem. C*, 2010, **114**, 19582–19595.

16 S. Malola, S. Svelle, F. L. Bleken and O. Swang, Detailed reaction paths for zeolite dealumination and desilication from density functional calculations, *Angew. Chem., Int. Ed.*, 2012, **51**, 652–655.

17 M. C. Silaghi, C. Chizallet, E. Petracovschi, T. Kerber, J. Sauer and P. Raybaud, Regioselectivity of Al–O bond hydrolysis during zeolites dealumination unified by Brønsted-Evans-Polanyi relationship, *ACS Catal.*, 2015, **5**, 11–15.

18 K. Stanciakova, B. Ensing, F. Göltl, R. E. Bulo and B. M. Weckhuysen, Cooperative role of water molecules during the initial stage of water-induced zeolite dealumination, *ACS Catal.*, 2019, **9**, 5119–5135.

19 M. C. Silaghi, C. Chizallet, J. Sauer and P. Raybaud, Dealumination mechanisms of zeolites and extra-framework aluminum confinement, *J. Catal.*, 2016, **339**, 242–255.

20 T. Fjermestad, S. Svelle and O. Swang, Mechanistic comparison of the dealumination in SSZ-13 and the desilication in SAPO-34, *J. Phys. Chem. C*, 2013, **117**, 13442–13451.

21 M. Nielsen, R. Y. Brogaard, H. Falsig, P. Beato, O. Swang and S. Svelle, Kinetics of zeolite dealumination: insights from H-SSZ-13, *ACS Catal.*, 2015, **5**, 7131–7139.

22 K. Stanciakova, J. N. Louwen, B. M. Weckhuysen, R. E. Bulo and F. Göltl, Understanding water-zeolite interactions: on the accuracy of density functionals, *J. Phys. Chem. C*, 2021, **125**, 20261–20274.

23 M. Nielsen, A. Hafreager, R. Y. Brogaard, K. De Wispelaere, H. Falsig, P. Beato, V. Van Speybroeck and S. Svelle, Collective action of water molecules in zeolite dealumination, *Catal. Sci. Technol.*, 2019, **9**, 3721–3725.

24 L. Shi, J. Yang, G. Shen, Y. Zhao, R. Chen, M. Shen, Y. Wen and B. Shan, The influence of adjacent Al atoms on the hydrothermal stability of H-SSZ-13: a first-principles study, *Phys. Chem. Chem. Phys.*, 2020, **22**, 2930–2937.

25 T. Nishitoba, N. Yoshida, J. N. Kondo and T. Yokoi, Control of Al distribution in the CHA-type aluminosilicate zeolites and its impact on the hydrothermal stability and catalytic properties, *Ind. Eng. Chem. Res.*, 2018, **57**, 3914–3922.

26 B. Arstad, A. Lind, J. H. Cavka, K. Thorshaug, D. Akporiaye, D. Wragg, H. Fjellvåg, A. Grønvold and T. Fuglerud, Structural changes in SAPO-34 due to hydrothermal treatment. a NMR, XRD, and DRIFTS study, *Microporous Mesoporous Mater.*, 2016, **225**, 421–431.

27 G. N. Kalantzopoulos, F. Lundvall, K. Thorshaug, A. Lind, P. Vajeeston, I. Dovgaliuk, B. Arstad, D. S. Wragg and H. Fjellvåg, Factors determining microporous material stability in water: the curious case of SAPO-37, *Chem. Mater.*, 2020, **32**, 1495–1505.

28 J. Holzinger, P. Beato, L. F. Lundegaard and J. Skibsted, Distribution of aluminum over the tetrahedral sites in ZSM-5 zeolites and their evolution after steam treatment, *J. Phys. Chem. C*, 2018, **122**, 15595–15613.

29 J. Barras, J. Klinowski and D. W. McComb, 27Al and 29Si solid-state NMR studies of dealuminated mordenite, *J. Chem. Soc., Faraday Trans.*, 1994, **90**, 3719–3723.

30 G. N. Kalantzopoulos, F. Lundvall, S. Checchia, A. Lind, D. S. Wragg, H. Fjellvåg and B. Arstad, In situ flow MAS NMR spectroscopy and synchrotron PDF Analyses of the local response of the brønsted acidic site in SAPO-34 during hydration at elevated temperatures, *ChemPhysChem*, 2018, **19**, 519–528.

31 G. Agostini, C. Lamberti, L. Palin, M. Milanesio, N. Danilina, B. Xu, M. Janousch and J. A. Van Bokhoven, In situ XAS and XRPD parametric rietveld refinement to understand dealumination of Y zeolite catalyst, *J. Am. Chem. Soc.*, 2010, **132**, 667–678.

32 J. A. Van Bokhoven, A. M. J. Van der Eerden and D. C. Koningsberger, Three-coordinate aluminum in zeolites observed with in situ X-ray absorption near-ddge spectroscopy at the Al K-edge: flexibility of aluminum coordinations in zeolites, *J. Am. Chem. Soc.*, 2003, **125**, 7435–7442.

33 A. Vjunov, M. A. Derewinski, J. L. Fulton, D. M. Camaioni and J. A. Lercher, Impact of zeolite aging in hot liquid water on activity for acid-catalyzed dehydration of alcohols, *J. Am. Chem. Soc.*, 2015, **137**, 10374–10382.

34 G. L. Woolery and G. H. Kuehl, On the nature of framework brønsted and lewis acid sites in ZSM-5, *Zeolites*, 1997, **19**, 288–296.

35 K. Chen, S. Horstmeier, V. T. Nguyen, B. Wang, S. P. Crossley, T. Pham, Z. Gan, I. Hung and J. L. White, Structure and catalytic characterization of a second framework Al(IV) site in zeolite catalysts revealed by NMR at 35.2 T, *J. Am. Chem. Soc.*, 2020, **142**, 7514–7523.

36 K. Chen, Z. Gan, S. Horstmeier and J. L. White, Distribution of aluminum species in zeolite catalysts: 27Al NMR of framework, partially-coordinated framework, and non-framework moieties, *J. Am. Chem. Soc.*, 2021, **143**, 6669–6680.

37 M. Ravi, V. L. Sushkevich and J. A. van Bokhoven, On the location of lewis acidic aluminum in zeolite mordenite and the role of framework-associated aluminum in mediating the switch between brønsted and lewis acidity, *Chem. Sci.*, 2021, **12**, 4094–4103.

This journal is © the Partner Organisations 2022

Inorg. Chem. Front., 2022, **9**, 3609–3618 | **3617**

38 U. Lohse, E. Löffler, M. Hunger, J. Stöckner and V. Patzelová, Hydroxyl groups of the non-framework aluminium species in dealuminated Y zeolites, *Zeolites*, 1987, **7**, 11–13.

39 R. D. Shannon, K. H. Gardner, R. H. Staley, G. Bergeret, P. Gallezot and A. Auroux, The nature of the nonframework aluminum species formed during the dehydroxylation of H-Y, *J. Phys. Chem.*, 1985, **89**, 4778–4788.

40 D. L. Bhering, A. Ramírez-Solís and C. J. A. Mota, A Density functional theory based approach to extraframework aluminum species in zeolites, *J. Phys. Chem. B*, 2003, **107**, 4342–4347.

41 S. Li, A. Zheng, Y. Su, H. Zhang, L. Chen, J. Yang, C. Ye and F. Deng, Brønsted/lewis acid synergy in dealuminated HY zeolite: A combined solid-state NMR and theoretical calculation study, *J. Am. Chem. Soc.*, 2007, **129**, 11161–11171.

42 Z. Yu, A. Zheng, Q. Wang, L. Chen, J. Xu, J.-P. Amoureux and F. Deng, Insights into the dealumination of zeolite HY revealed by sensitivity-enhanced 27Al DQ-MAS NMR spectroscopy at high field, *Angew. Chem.*, 2010, **122**, 8839–8843.

43 C. Liu, G. Li, E. J. M. Hensen and E. A. Pidko, Nature and catalytic role of extraframework aluminum in faujasite zeolite: a theoretical perspective, *ACS Catal.*, 2015, **5**, 7024–7033.

44 X. Yi, K. Liu, W. Chen, J. Li, S. Xu, C. Li, Y. Xiao, H. Liu, X. Guo, S. B. Liu and A. Zheng, Origin and structural characteristics of tri-coordinated extra-framework aluminum species in dealuminated zeolites, *J. Am. Chem. Soc.*, 2018, **140**, 10764–10774.

45 S. Xin, Q. Wang, J. Xu, Y. Chu, P. Wang, N. Feng, G. Qi, J. Trébosc, O. Lafon, W. Fan and F. Deng, The acidic nature of 'NMR-invisible' tri-coordinated framework aluminum species in zeolites, *Chem. Sci.*, 2019, **10**, 10159–10169.

46 Z. Wang, L. A. O'Dell, X. Zeng, C. Liu, S. Zhao, W. Zhang, M. Gaborieau, Y. Jiang and J. Huang, Insight into three–coordinate aluminum species on ethanol–to–olefin conversion over ZSM–5 Zeolites, *Angew. Chem.*, 2019, **131**, 18229–18236.

47 J. A. Van Bokhoven, D. C. Koningsberger, P. Kunkeler, H. Van Bekkum and A. P. M. Kentgens, Stepwise dealumination of zeolite beta at specific T-Sites observed with 27Al MAS and 27Al MQ MAS NMR, *J. Am. Chem. Soc.*, 2000, **122**, 12842–12847.

48 D. Coster, A. L. Blumenfeld, J. J. Fripiat, H. M. Kao, C. P. Grey, G. A. Morris and R. Freeman, Determination of the 31P–27Al J-coupling constant for trimethylphosphine bound to the lewis acid site of zeolite HY, *J. Am. Chem. Soc.*, 1997, **119**, 627–628.

49 L. Wang, D. Zhu, J. Wang, W. Cui, J. Han, B. Li, D. Fan, P. Tian and Z. Liu, Embryonic zeolite-assisted synthesis of SSZ-13 with superior efficiency and their excellent catalytic performance, *J. Mater. Chem. A*, 2021, **9**, 15238–15245.

50 J. Wang, L. Wang, D. Zhu, W. Cui, P. Tian and Z. Liu, One-pot synthesis of Na$^+$-free Cu-SSZ-13 and its application in the NH$_3$–SCR reaction, *Chem. Commun.*, 2021, **57**, 4898–4901.

51 M. Lusardi, T. T. Chen, M. Kale, J. H. Kang, M. Neurock and M. E. Davis, Carbonylation of dimethyl ether to methyl acetate over SSZ-13, *ACS Catal.*, 2020, **10**, 842–851.

52 T. H. Chen, K. Houthoofd and P. J. Grobet, Toward the aluminum coordination in dealuminated mordenite and amorphous silica–alumina: a high resolution 27Al MAS and MQ MAS NMR study, *Microporous Mesoporous Mater.*, 2005, **86**, 31–37.

53 D. E. Akporiaye, I. M. Dahl, H. B. Mostad and R. Wendelbo, Aluminum distribution in chabazite: an experimental and computational study, *J. Phys. Chem.*, 1996, **100**, 4148–4153.

54 J. R. Di Iorio and R. Gounder, Controlling the isolation and pairing of aluminum in chabazite zeolites using mixtures of organic and inorganic structure-directing agents, *Chem. Mater.*, 2016, **28**, 2236–2247.

55 X. Zhu, N. Kosinov, J. P. Hofmann, B. Mezari, Q. Qian, R. Rohling, B. M. Weckhuysen, J. Ruiz-Martínez and E. J. M. Hensen, Fluoride-assisted synthesis of bimodal microporous SSZ-13 zeolite, *Chem. Commun.*, 2016, **52**, 3227.

56 X. Zhu, J. P. Hofmann, B. Mezari, N. Kosinov, L. Wu, Q. Qian, B. M. Weckhuysen, S. Asahina, J. Ruiz-Martínez and E. J. M. Hensen, Trimodal porous hierarchical SSZ-13 zeolite with improved catalytic performance in the methanol-to-olefins reaction, *ACS Catal.*, 2016, **6**, 2163–2177.

57 K. Mlekodaj, J. Dedecek, V. Pashkova, E. Tabor, P. Klein, M. Urbanova, R. Karcz, P. Sazama, S. R. Whittleton, H. M. Thomas, A. V. Fishchuk and S. Sklenak, Al Organization in the SSZ-13 zeolite. Al distribution and extraframework sites of divalent cations, *J. Phys. Chem. C*, 2019, **123**, 7968–7987.

58 K. Chen, M. Abdolrhamani, E. Sheets, J. Freeman, G. Ward and J. L. White, Direct detection of multiple acidic proton sites in zeolite HZSM-5, *J. Am. Chem. Soc.*, 2017, **139**, 18698–18704.